Synthesis and Thermal Properties of Ferroelectric Side Chain Liquid Crystalline Polysiloxanes Based on the Phenyl Ester Mesogen and Oligo(oxyethylene) Spacers. 1. Phenyl Benzoate and Biphenyl Benzoate Mesogenic Groups

Ging-Ho Hsiue* and Jr-Hong Chen

Department of Chemical Engineering, National Tsing Hua University, Hsinchu, Taiwan 300, R.O.C.

Received January 6, 1995; Revised Manuscript Received April 4, 1995[⊗]

ABSTRACT: Four series of ferroelectric side chain polysiloxanes containing oligo(oxyethylene) spacers and (2*S*)-2-methyl-1-butyl 4-(((4-hydroxyphenyl)carbonyl)oxy)benzoate, (2*S*)-2-methyl-1-butyl 4′-(((4-hydroxyphenyl)carbonyl)oxy)-1,1′-biphenyl-4-carboxylate, (2*R*)-1-methylheptyl 4′-(((4-hydroxyphenyl)-carbonyl)oxy)-1,1′-biphenyl-4-carboxylate, and 4-[(2*S*, 3*S*)-(2-chloro-3-methylpentanoyl)oxy]-1,1′-biphenyl-4′-yl benzoate mesogenic groups were synthesized. The mesomorphic behavior of the four series of ferroelectric side chain liquid crystalline polysiloxanes are studied in this work using differential scanning calorimetry, optical polarizing microscopy, and high-resolution X-ray diffraction measurements. Some of these side chain polysiloxanes containing three phenyl rings of ester cores (i.e., −Ph−COO−Ph−Ph−) and a chiral butyl tail present a rich mesomorphic behavior: a blue phase (BP), a cholesteric phase (N*), a smectic A (S_A) phase, a twist grain boundary A (TGB_A) phase, a chiral smectic F (S_F*) phase, and a chiral smectic C (Sc*) phase over a wide temperature range (around 160 °C). Another series containing three phenyl rings of ester cores and a chiral heptyl chain tail only reveal the S_A phase and TGB_A phase. The intermediary twist grain boundary phase would display an iridescent Grandjean plane or a filament texture. Results obtained in this study seem to imply that the tendency toward chiral smectic C mesomorphism increases as the rigidity of phenyl ester mesogens increases via the flexible oligo-(oxyethylene) spacer system, and the thermal stability of the chiral smectic C mesophase is determined by the flexibility of the chiral tail.

Introduction

In 1975 Meyer *et al.*[1] presented theoretically and then proved experimentally that the Sc* mesophase is ferroelectric. Prompted by the development of the surface-stabilized ferroelectric liquid crystal (SSFLC) display technology by Clark and Lagerwall,[2] the ferroelectric properties (e.g., bistability, spontaneous polarization (Ps), response time (τ), and tilt angle (θ)) and technology of the ferroelectric liquid crystal (FLC) cell were extensively investigated.[3−6] Thus, great strides have been made toward the realization and application of practical devices.[7,8] For FLC display devices, it is desirable that a FLC material show a chiral smectic C phase over a wide temperature range including room temperature. Moreover, the liquid crystal material is required to possess a large spontaneous polarization. Consequently, a FLC-related device can be operated at a reduced driving voltage. These properties are influenced by the molecular structures of the liquid crystal compounds. An increasing interest in the synthesis of low molar mass Sc* liquid crystals has since then developed. Numerous FLC compounds and room temperature mixtures have so far been prepared for fast electrooptical applications. Besides low molar mass FLCs, several side chain liquid crystalline polymers (LCPs) exhibiting a Sc* mesophase and their ferroelectric properties have been reported during the past few years.[9−25] The field was thoroughly reviewed by LeBarney and Dubois.[26] However, the detailed relationship between the structure and the properties of Sc* LCPs remains unclear as the result of the limited experimental data reported in the literature. As a part of the research program dedicated to the development of high-efficiency FLC materials, novel low molar mass FLCs and ferroelectric side chain liquid crystalline polymers have been designed and synthesized in our group.[27,28] They exhibit a broad temperature range of the chiral smectic C phase and satisfactory electrooptical properties.[29] In this study, several new series of ferroelectric side chain liquid crystalline polysiloxanes containing oligo(oxyethylene) spacers, phenyl benzoate/biphenyl benzoate mesogens, and three different kinds of chiral moieties ((2*S*)-2-methyl-1-butyl, (2*R*)-1-methylheptyl, and (2*S*,3*S*)-(2-chloro-3-methylpentanoyl)oxy) are synthesized. Their characterizations by differential scanning calorimetry, optical polarizing microscopy, and high-resolution X-ray diffraction measurements are also presented.

Experimental Section

A. Materials. Allyl bromide, 2-chloroethanol, 2-(2-chloroethoxy)ethanol, 2-(2-(2-chloroethoxy)ethoxy)ethanol, 4-hydroxy-4′-biphenylcarboxylic acid (from Aldrich); methyl 4-hydroxybenzoate, 4-hydroxybenzoic acid, 4,4′-dihydroxybiphenyl (from TCI); (2*S*)-2-methyl-1-butanol (from Fluka); L-2-octanol (from Janssen); and L-isoleucine and other reagents (from Merk) were used as received. Poly(methylhydrosiloxane) ($\bar{M}_n = 2270$) and (divinyltetramethyldisiloxane)platinum catalyst were obtained from Hüls Inc. and used as received. Toluene used in the hydrosilation reaction was dried over sodium and then distilled under nitrogen.

B. Techniques. ^{1}H-NMR spectra were recorded on a Bruker AM300 spectrometer. FT-IR spectra were measured on a Bio-Rad FTS-155 spectrometer. Polymer samples were cast as films on a KBr tablet for the measurement. A Seiko DSC 220C/5200H differential scanning calorimeter equipped with a liquid nitrogen cooling accessory was used to determine the thermal transitions and thermodynamic parameters. Heating and cooling rates were 10 °C min^{-1}. The thermal transitions reported were collected during the second heating

* To whom all correspondence should be addressed.
[⊗] Abstract published in *Advance ACS Abstracts,* May 15, 1995.

0024-9297/95/2228-4366$09.00/0

Table 1

(a) Transition Temperatures for the Series MD*n*11A and MD*n*12A[30]

name	n^a	$[\alpha]_D^{25}$	heating / cooling (corresponding enthalpy changes, kcal/mol)
MD011A	0	+2.94	K 48.52(−) S_A 50.92(4.12)[b] I / I 25(−) S_A 21.65(−) S 18.84(5.44)[c] K
MD111A	1	+2.66	K 16.62(0.25) S 38.43(4.97) I / I 23.09(5.05) S 15.5(0.196) K
MD211A	2	+1.98	K − [d] *I* / I − [d] *K*
MD311A	3	+1.567	K − [d] *I* / I − [d] *K*
MD012A	0	+2.57	K 97.8(6.2) S_A 144(0.272) Ch 180(0.13) I / I 180 BP 178(0.14) Ch 136(0.27) S_A 54.4(4.78) K
MD112A	1	+2.203	K 71.4(4.54) Sc* 95(0.07) S_A 127.2(0.18) Ch 145.1(0.12) I / I 151.9 BP 144(0.1)[e] Ch 126.6(0.14)[f] TGB_A 125.7(−) S_A 93(0.09) Sc* 1.5(2.32) K
MD212A	2	+1.513	K 62.4(7.8) Sc* 79(0.11) S_A 93.5(0.29) Ch 107.5(0.14) I / I 108.4 BPII 106.3 BPI 106(0.11)[g] Ch 94.9(0.25)[f] TGB_A 93.3(−) S_A 78(0.13) Sc* −8.5(2.128) K
MD312A	3	+1.463	K 19.5(−) Sc* 49.5(0.082) S_A 57.4(0.164) Ch 71.4(0.096) I / I 69 BPII 67.3 BPI 60.5(0.082)[g] Ch 55(0.164)[f] TGB_A 51.2(−) S_A 49(0.15) Sc* −42.3(−)[h] K

(b) Transition Temperatures for the Series MD*n*12B and MD*n*12C[30]

name	n^a	$[\alpha]_D^{25}$	heating / cooling (corresponding enthalpy changes, kcal/mol)
MD012B	0	+26.744	K 84.7(4.89) S_A 136.9(1.19) I / I 133.3(1.16) S_A 33.51(2.23) K
MD112B	1	+25.92	K 65.5(4.95)[i] Sc* 69.1(−) S_A 104.1(0.69) I / I 101.9(0.65) S_A 27.5(−) Sc* 24.3(2.85)[i] K
MD212B	2	+23.28	K 72.54(7.38) I / I 58.4(0.675) S_A 28(5.09) Sc* 26.7 K
MD312B	3	+21.59	K −40(0.08) S_1 −14.11(0.03) S_2 −7.1(0.04) S_3 19.72(0.56) I / I 20.8(−) S_A 16.48(0.59)[j] S_3 −4.7(0.059) S_2 −12.76(0.03) S_1 −46.05(−) K
MD012C	0	−3.012	K 78.9(2.26) S_A 100(0.11) Ch 181.7(0.09) I / I 179.5 BP 178(0.16) Ch 92.3(0.13)[f] TGB_A 84.3(−) S_A 67.5(1.8) K
MD112C	1	−3.423	K 29.9(0.92) S 57.1(0.174) Sc* 113.2(0.89) Ch 141.7(0.11) I / I 142.2 BPII 141.8 BPI 136(0.13) Ch 112.1(0.91) Sc* 53.9(0.23) S 23.9(0.124) K
MD212C	2	−7.523	K −9.2(0.57) Sc* 88.3(0.98) Ch 103.5(0.108) I / I 102 BPII 96.6 BPI 90.2(0.243) Ch 85.9(1.05) Sc* −13.9(0.78) K
MD312C	3	−5.889	K −25.26(−)[h] Sc* 57.59(0.77) BP 63.5(0.03) I / I 63.77(0.04) BP 58.6(0.77) Sc* −28.13(−)[h] K

[a] *n* according to Scheme 1. [b] ΔH(K−S_A−I). [c] ΔH(I−S_A−S−K). [d] No liquid crystalline phase was observed and the melting point was below −20 °C. [e] ΔH(I−BP−Ch). [f] ΔH(Ch−TGB_A−S_A). [g] ΔH(I−BPII−BPI−Ch). [h] Enthalpies were too small to be evaluated. [i] ΔH(K−Sc*−S_A). [j] ΔH(I−S_A−S_3).

and cooling scans. A Nikon Microphot-FX optical polarized microscope equipped with a Mettler an FP-80 hot stage and FP-82 central processor was used in observing the thermal transitions and anisotropic textures. An applied Biosystem 200 instrument equipped with a Viscotek differential refractometer and a preparative GPC column (22.5 mm × 60 cm) supplied by American Polymer Standard Co. was used. X-ray diffraction measurements were performed with a Rigaku R-Axis IIC powder diffractometer. Two imaging plate (abbreviated IP) detectors were used so that reflection spot exposure and readout operations could be performed. This feature provides increased data collection efficiency and minimizes the time required for IP residual image erasure. The monochromatized X-ray beam from nickel-filtered Cu Kα radiation with a wavelength of 0.15406 nm was used. A temperature controller was added to the X-ray apparatus for thermal measurements. The precision of the controller was ±0.5 °C in the temperature range studied. Optical rotations were measured at 25 °C on a Jasco DIP-140 polarimeter with chloroform as solvent for all compounds.

Scheme 1. Synthesis of Monomer Series MD*n*11A, MD*n*12A, MD*n*12B, and MD*n*12C

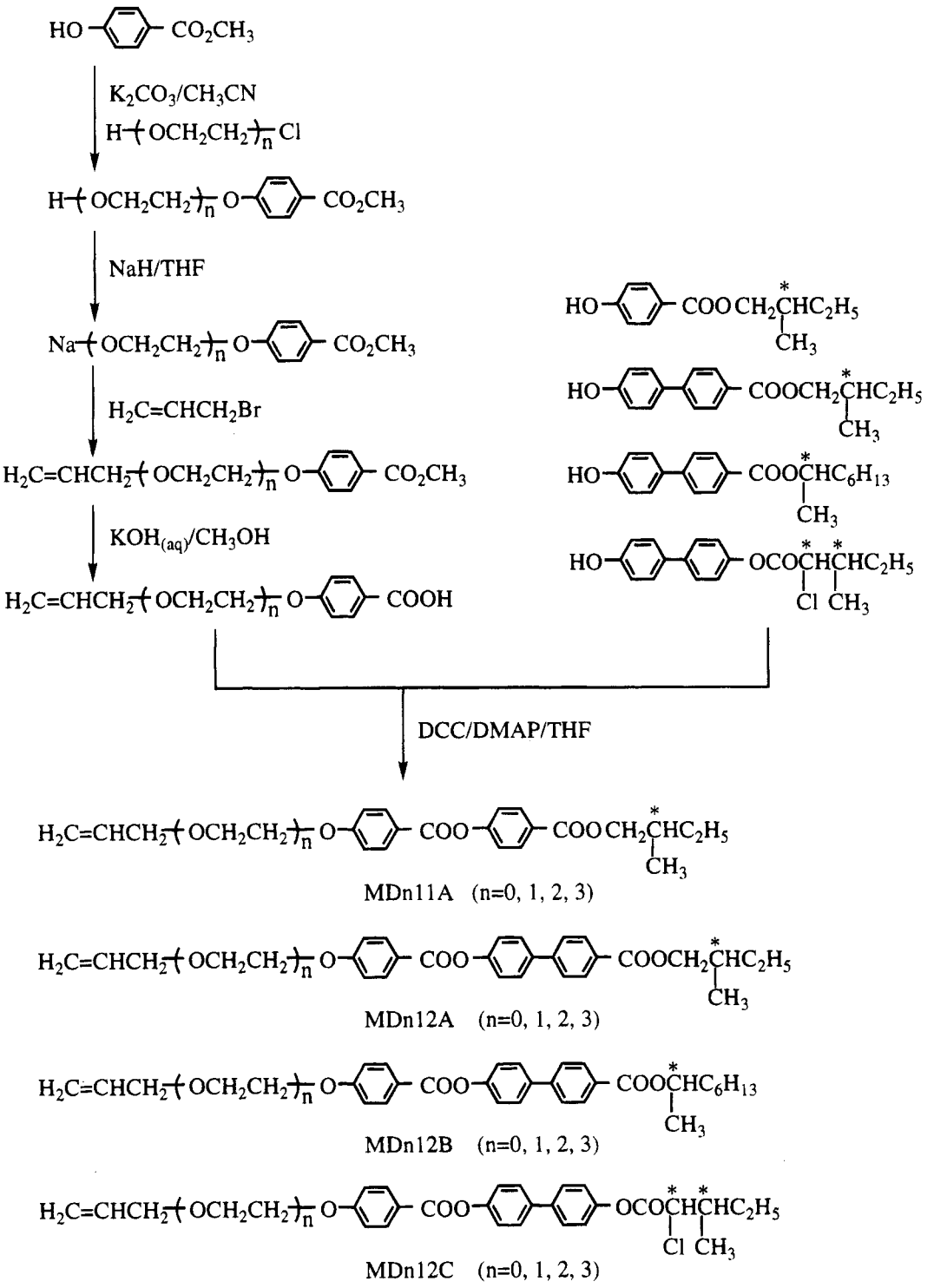

C. Synthesis of Monomers. The synthesis of olefin monomers, series MD*n*11A, MD*n*12A, MD*n*12B, and MD*n*12C, for the hydrosilation reaction have been described previously.[30] The optical rotations, $[\alpha]_D^{25}$, of these monomers are summarized in Table 1.

D. Synthesis of Polysiloxane Series PS*n*11A, PS*n*12A, PS*n*12B, and PS*n*12C. The synthesis of liquid crystalline polysiloxanes is outlined in Scheme 2. A general synthetic procedure is described below.

The olefin derivative, 0.5 g (10 mol % excess versus the Si–H groups present in the polysiloxanes), was dissolved in 50 mL of dry, freshly distilled toluene together with the proper amount of poly(methylhydrosiloxane). The reaction mixture was heated to 110 °C under nitrogen. Next 100 μg of (divinyltetramethyldisiloxane)platinum catalyst was then injected with a syringe as a solution in toluene (1 mg/mL). The reaction mixture was refluxed (110 °C) under nitrogen for 24 h. After this reaction time, FT-IR analysis indicated that the hydrosilation reaction was complete. The polymers were separated and purified by several reprecipitations from tetrahydrofuran solution into methanol, further purified by preparative GPC, and then dried under vacuum.

Results and Discussion

The synthetic route for the preparation of allyl monomers (series MD*n*11A, MD*n*12A, MD*n*12B, and MD*n*12C) is outlined in Scheme 1. The detailed synthetic method of these ester compounds has been reported elsewhere.[30] Table 1 summarizes the thermal

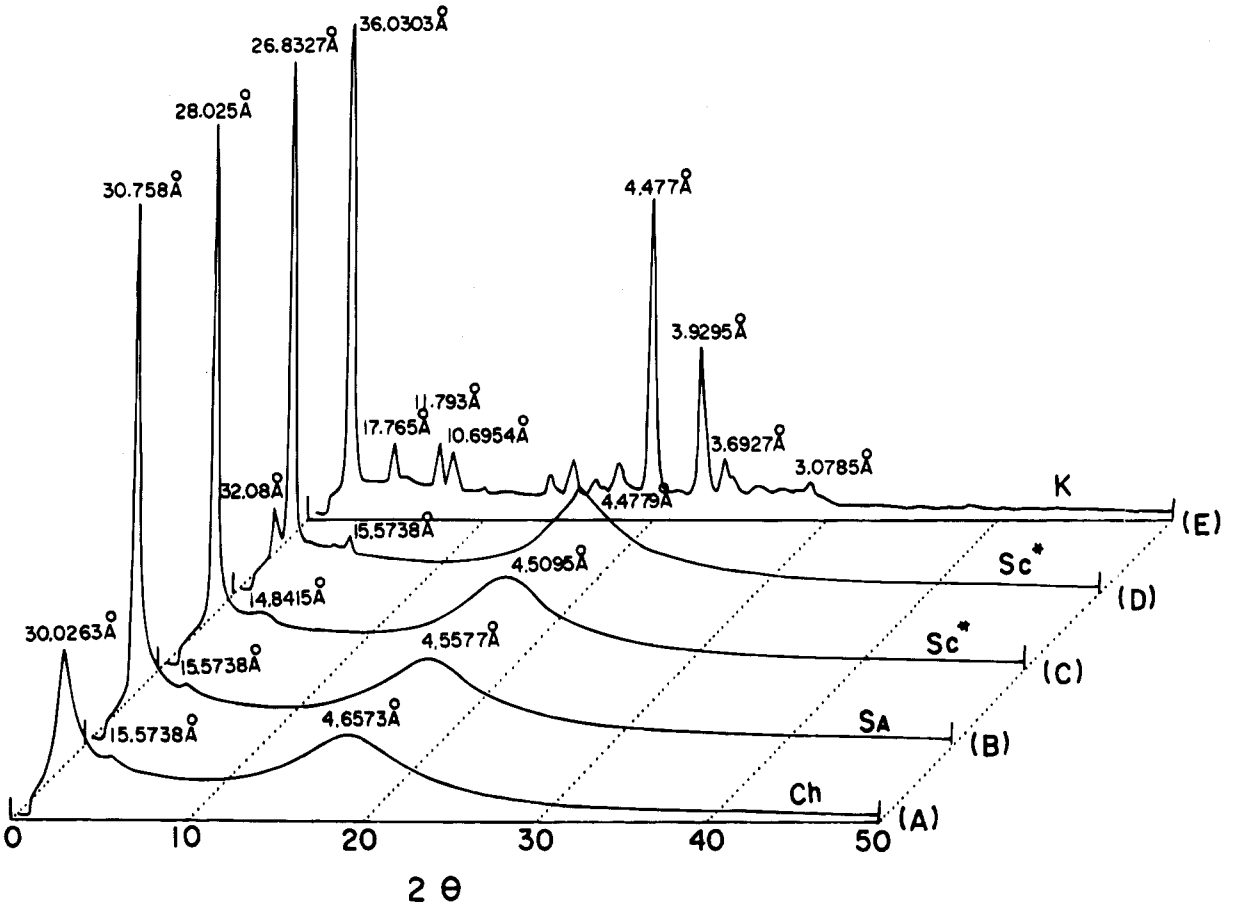

Figure 1. Temperature-dependent X-ray diffraction measurements for MD212A at (A) 100, (B) 85, (C) 70, (D) 25, and (E) 23.4 °C.

transition and corresponding enthalpy changes of the monomer series MD*n*11A, MD*n*12A, MD*n*12B, and MD*n*12C. The mesomorphism of these monomers was again confirmed by high-resolution X-ray diffraction measurements. A representative temperature dependence of the X-ray diffraction measurements for powder monomer MD212A ($n = 2$) at 100, 85, 70, 25, and 23.4 °C is presented in Figure 1.

The synthesis of the polymer series PS*n*11A, PS*n*12A, PS*n*12B, and PS*n*12C is described in Scheme 2. An excess of olefin monomers was usually used to carry the hydrosilation reaction to completion. The unreacted monomers were removed by several reprecipitations from chloroform solution into methanol and by preparative GPC. Therefore, the polymers were isolated with high purity.

Series PS*n*11A. This series was composed of the (2*S*)-2-methyl-1-butyl 4-(((4-hydroxyphenyl)carbonyl)-oxy)benzoate mesogen and oxyethylene spacer units. However, these compounds behave as a viscous liquid and exhibit no mesophase.

Series PS*n*12A. This series contained the (2*S*)-2-methyl-1-butyl 4′-(((4-hydroxyphenyl)carbonyl)oxy)-1,1′-biphenyl-4-carboxylate mesogenic side group and oxyethylene spacers. The biphenyl ring in the mesogen core revealed a richer mesomorphic behavior as compared to the series PS*n*11A (see Figure 2a). Table 2 summarizes the thermal transitions and thermodynamic parameters of the obtained polymer PS*n*12A series. All four polymers present a smectic mesomorphism. PS012A shows enantiotropic N*, TGB_A, and Sc* phases. Both PS112A and PS212A exhibit enantiotropic N*, S_A, Sc*, and S_F* phases. Meanwhile, polymer PS312A exhibits enantiotropic S_A and Sc* phases. The phase assignment was made by optical polarizing microscopic observation and X-ray diffraction measurements. Figure 3 presents the temperature-dependent X-ray diffraction diagrams obtained from a powder sample of PS112A at 199, 192, 180, and 27 °C. A broad reflection at wide angles (associated with the lateral packings) and a sharp reflection at small angles (associated with the smectic layers) are shown by all curves. Curve A exhibits a rather diffuse reflection at around 4.99 Å, which corresponds to the lateral spacing of two mesogenic side groups, and a very weak reflection at 31.0275 Å, which corresponds to a weak smectic layer structure. The optical polarizing micrograph (Figure 4a) reveals a quasi focal-conic texture for polymer PS112A at 200 °C. These results correlate with a cholesteric phase. Curve B presents a diffuse reflection at around 4.88 Å, a sharp first-order reflection at 30.5127 Å, and a second-order reflection at 15.3327 Å, which corresponds to strong smectic layers. In this temperature range, the optical polarizing micrograph (Figure 4b) reveals a focal-conic fan texture. Both results are consistent with a smectic A structure. When the measuring temperature is lowered from 192 to 180 °C, the *d*-spacing of the first-order reflection decreases from 30.5127 to 30.428 Å (curve C). The temperature dependence of the layer spacing for series PS*n*12A ($n = 0, 1, 2, 3$) is presented in Figure 5a. As shown in this figure, the *d*-spacing decreases as the temperature decreases below the transition point of the S_A phase and TGB_A phase for

Scheme 2. Synthesis of Polymer Series PS*n*11A, PS*n*12A, PS*n*12B, and PS*n*12C

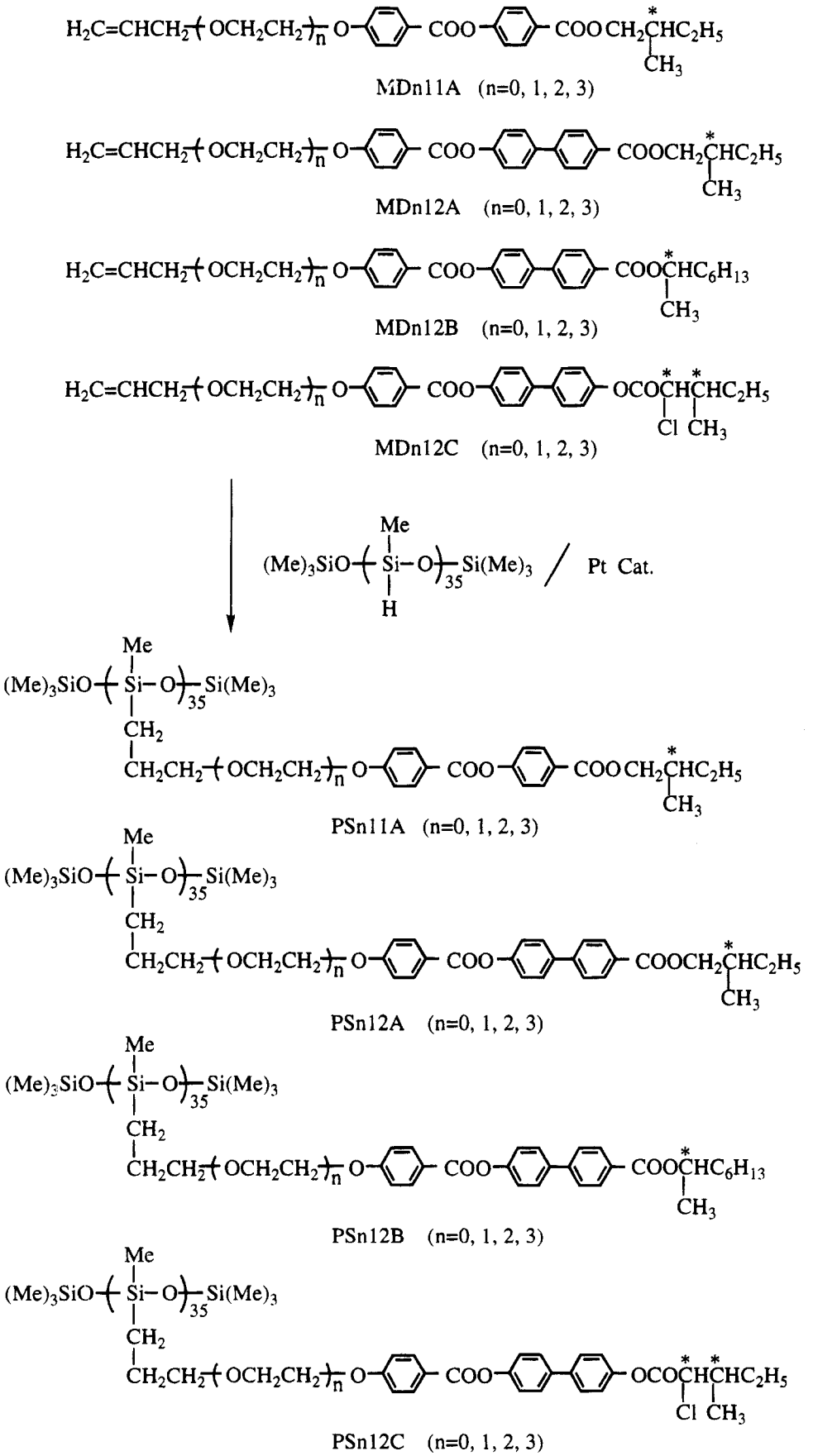

PS112A to PS312A ($n = 1-3$) and PS012A ($n = 0$). This phenomenon provides strong evidence for the formation of the tilted chiral smectic C phase. This result also correlates with the optical microscopic observation which shows a broken fan texture (Figure 4c). The tilt angle is plotted in Figure 6a as a function of temperature difference below the T_{Sc^*} point ($T - T_{Sc^*}$). The tilt angles were calculated from eq 1.

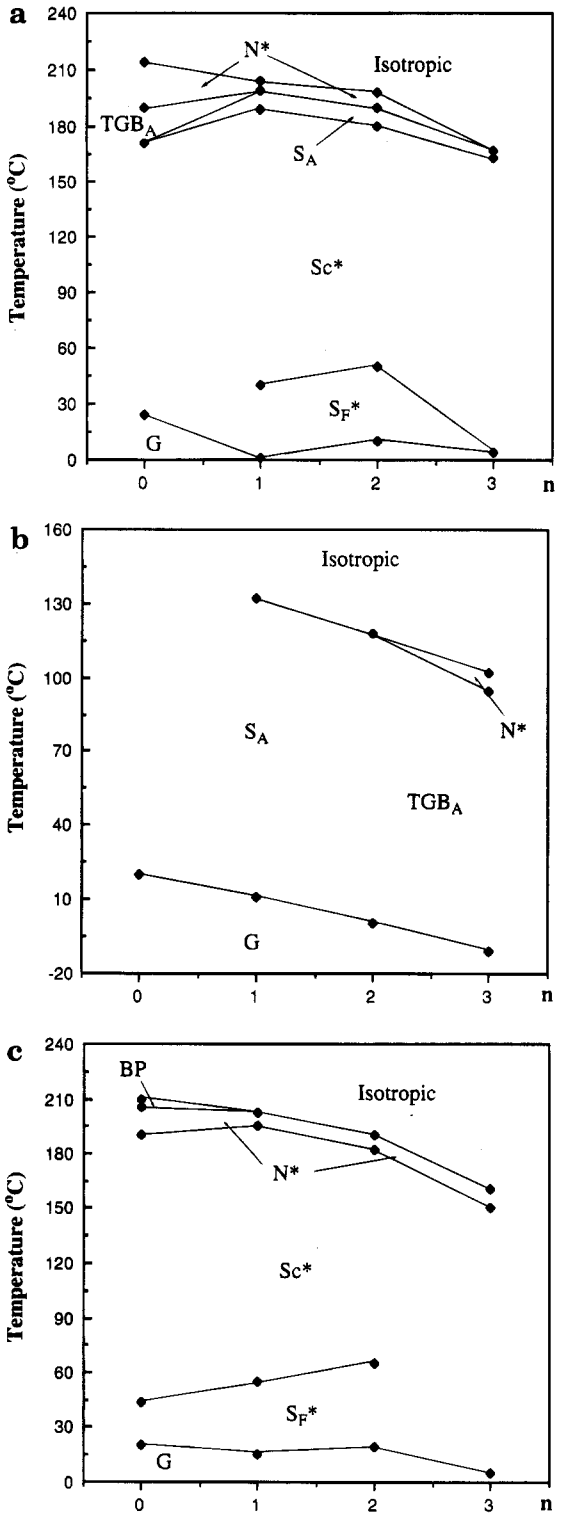

Figure 2. Plots of transition temperatures versus n, the number of oxyethylene spacer units: (a) series PSn12A; (b) series PSn12B; (c) series PSn12C.

$$\theta = \cos^{-1}\left(\frac{d_{Sc^*}}{d_{S_A}}\right) \quad (1)$$

The d_{S_A} value was selected from the maximum value of the layer spacing of the S_A phase. The maximum value of the tilt angle is about 21° for PS012A. Additionally, the tilt angle value descends as the spacer length of this series ascends. When the measuring temperature was further decreased to 27 °C, the d-spacing of the first-order reflection changed back to

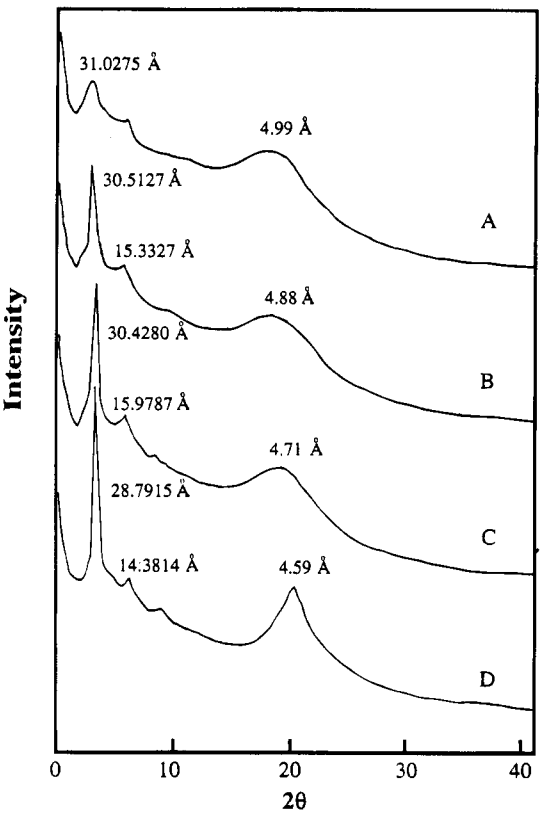

Figure 3. Temperature-dependent X-ray measurements for polymer PS112A at (A) 199, (B) 192, (C) 180, and (D) 27 °C.

28.7915 Å (Figure 5a) and the wide-angle reflection became sharp (curve D). These results are comparable to that observed in a chiral smectic F phase.[31] (Actually, in the absence of true monodomains of this biaxial phase, it is not really possible to distinguish whether this phase is of the smectic F or smectic I type. This comment also applies to all other smectic F phases mentioned in the following.) Figure 4d displays the chiral smectic F texture exhibited by PS112A. On the other hand, the X-ray diffraction measurements for PS012A show a smectic A-like diffraction pattern (a sharp reflection at small angles and a diffuse reflection at wide angles) at 190.5−171 °C. However, the optical polarizing micrograph reveals an iridescent cholesteric-like texture (Figure 7a). This texture can be distinguished from the cholesteric phase with oily streaks at a higher temperature (Figure 7b). One possible explanation for these results is that the special phase is a twist grain boundary A phase.[32-35]

Series PSn12B. This series differed structurally from the PSn12A series. The (2*S*)-2-methyl-1-butyl terminal chiral tail of PSn12A is replaced by the (2*R*)-1-methylheptyl chiral moiety. The thermal transition and corresponding enthalpy changes of the polymer PSn12B series are summarized in Table 3. All the polymers show a smectic mesomorphism except for PS012B with zero oxyethylene units, which shows an amorphous state and has no liquid crystalline phase. Both PS212B and PS312B exhibit an enantiotropic TGB_A phase, while PS112B reveals an enantiotropic smectic A phase. The cholesteric phase is exhibited between the isotropic and TGB_A phases for PS312B. Figure 8 presents representative DSC heating and cooling traces for polymer PS212B. The heating scan (curve A) indicates a glass transition (T_g) at −5 °C, followed by a twist grain boundary A phase to an isotropic phase at 122.7 °C. The cooling scan (curve B)

Table 2. Phase Transitions and Phase Transition Enthalpies for Polymer Series PS*n*11A and PS*n*12A

polymer	n^a	heating / cooling phase transitions, °C (corresponding enthalpy changes; kcal/mru)[b]
PS012A	0	G 27.4 Sc* –[d] TGB_A 192.1(–)[c] N* 217.8(0.288) I / I 213.6(0.276) N* 190.5(–)[c] TGB_A 171(–)[f] Sc* 24 G
PS112A	1	G 5.2 S_F* –[d] Sc* 190(–) S_A 199(–) N* 205.6(0.403)[e] I / I 204.2(–) N*198.9(–) S_A 189(0.64)[e] Sc* 40(–)[f] S_F* 1.2 G
PS212A	2	G 3.1 S_F* 40.4(0.14) Sc* 181(–) S_A 196.5(–) N* 201.4(0.775)[e] I / I 197.7(–) N*190.5(–) S_A 180(0.465)[e] Sc* 50(–)[f] S_F* 5.2G
PS312A	3	G 3.5 Sc* –[d] S_A 170.7(0.757) I / I 166.6(–) S_A 163.4(0.499)[g] Sc* 4.5 G

[a] *n* according to Scheme 2. [b] mru = mole repeating unit, G = glassy, S_F* = chiral smectic F, S_A = smectic A, Sc* = chiral smectic C, TGB_A = twist grain boundary A, N* = cholesteric, I = isotropic. [c] The transition was decided by POM. [d] The transition was difficult to detect. [e] ΔH (Sc*–S_A–N*–I). [f] The transition enthalpies were too small to evaluate. [g] ΔH(Sc*–S_A–I).

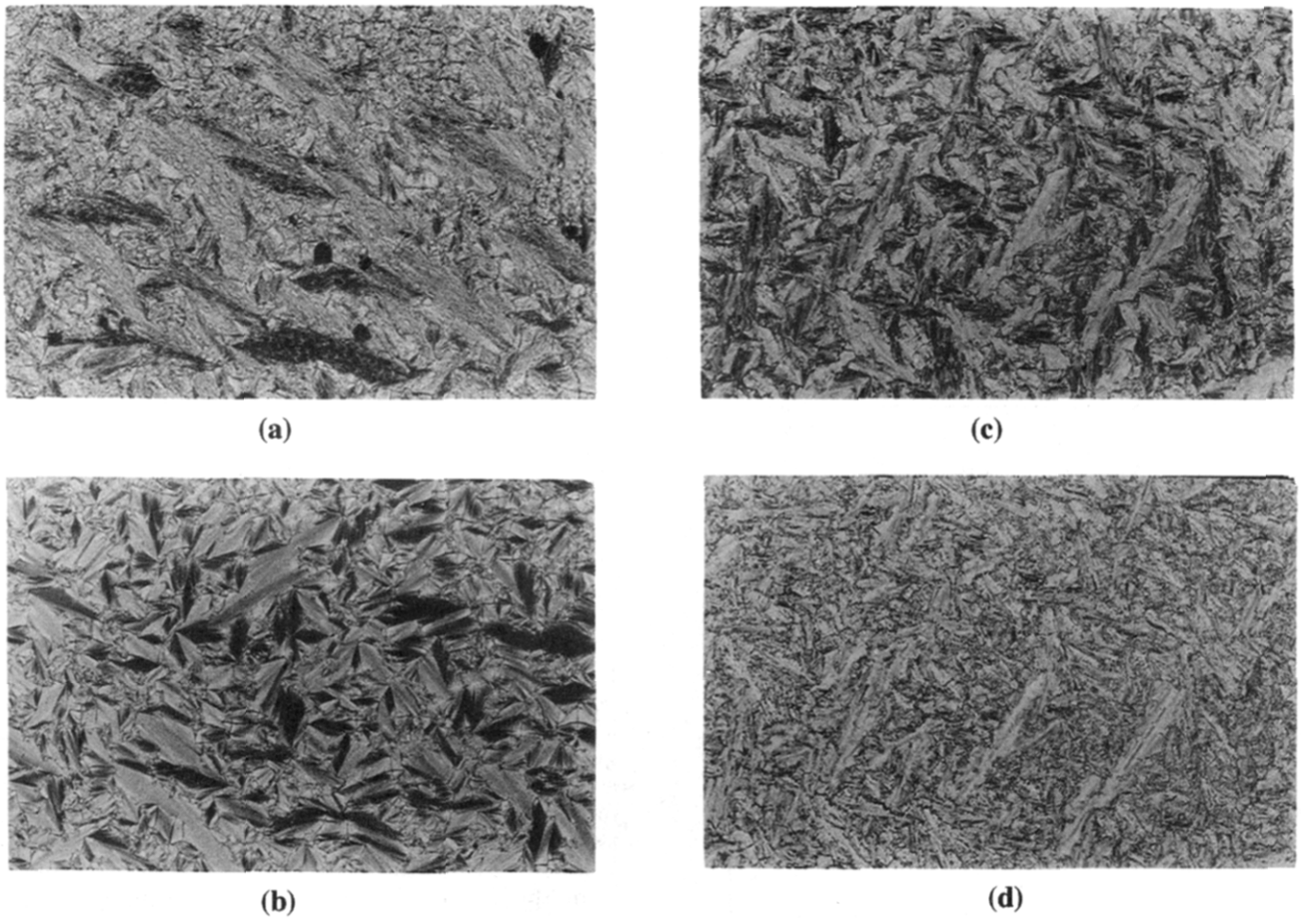

Figure 4. Optical polarizing micrographs displayed by PS112A: (a) cholesteric phase at 200 °C (400x); (b) focal-conic texture of smectic A phase at 192 °C (400x); (c) broken fan texture at 147 °C (400x); (d) chiral smectic F phase at 25 °C (400x).

is nearly identical to the heating scan. The presence of the TGB_A phase for two polymers was also proved by X-ray diffraction measurements and optical polarizing microscopy. Figure 9 shows representative temperature-dependent X-ray diffraction diagrams of the powder sample of PS212B at 103, 75, 61, and 25.6 °C. The diffraction patterns obtained at different temperatures resemble each other. A broad reflection at wide angles (associated with the random ordering of lateral packing) and a sharp reflection at low angles (associated with the smectic layers) are shown by all curves. Only the *d*-spacings are different. The d-spacing is plotted in Figure 5b as a function of temperature for the PS*n*12B series. As shown in this figure, the layer spacing increases with a decrease in the measuring temperature for PS212B.[35] Moreover, the filament texture displayed in Figure 10 indicates the presence of the twist grain boundary A phase because the macro helix is formed in the direction normal to the long axis of the molecules and parallel to the layers.[32–34]

Series PS*n*12C. The last series of compounds contained the (2*S*,3*S*)-(2-chloro-3-methylpentanoyl)oxy chiral moiety instead of the (2*S*)-2-methyl-1-butanoate and (2*R*)-1-methylheptanoate moieties of the PS*n*12A and PS*n*12B series. This type of moiety with two chiral centers has been reported to possess large spontaneous

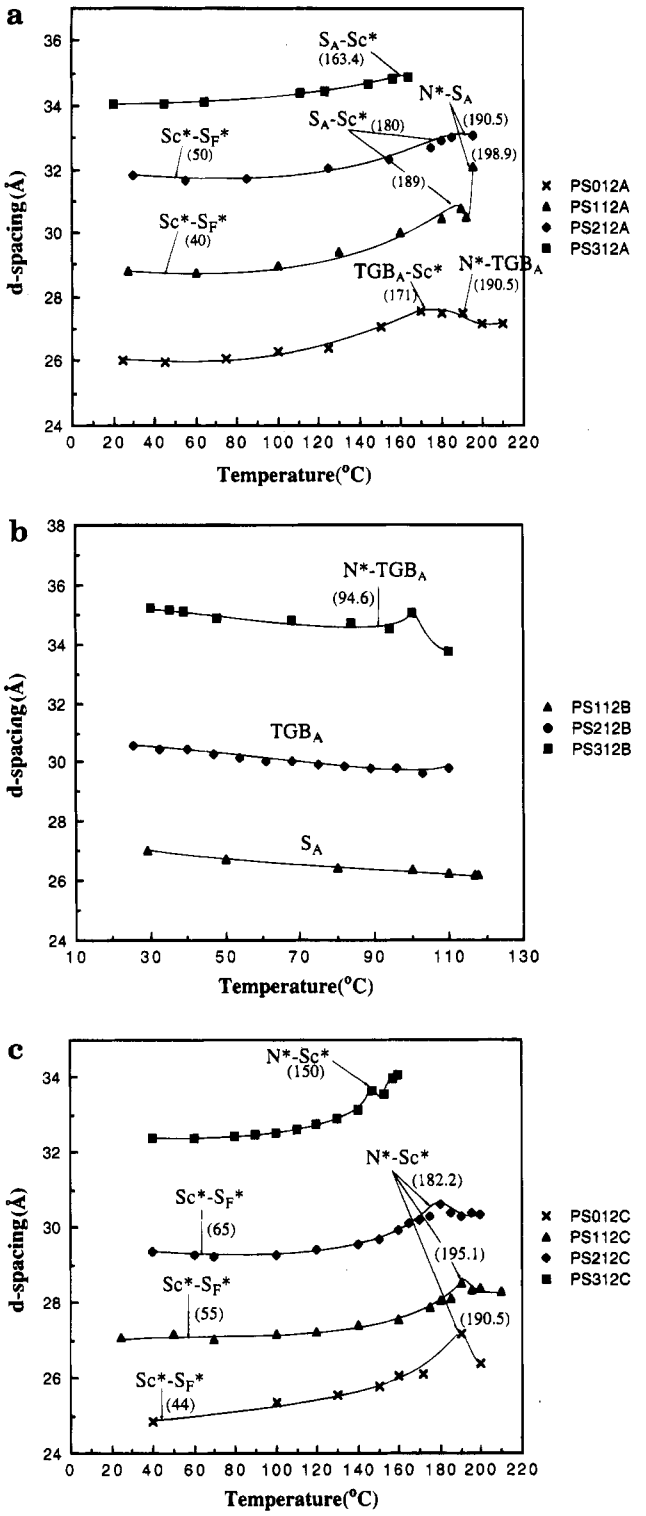

Figure 5. Temperature dependence of layer spacing: (a) series PSn12A, (n = 0, ×), (n = 1, ▲), (n = 2 , ◆), (n = 3 ■); (b) series PSn12B, (n = 1, ▲), (n = 2 , ◆), (n = 3, ■); (c) series PSn12C, (n = 0, ×), (n = 1, ▲), (n = 2, ◆), (n = 3, ■).

polarization values.[19] Four compounds of this series are all smectic mesomorphic. A different chiral moiety normally results in a different mesophasic sequence (see Figure 2c). The thermal transition and thermodynamic parameters of the PSn12C series are summarized in Table 4. The polymers exhibit glass transition temperatures (T_g) at 22.2, 20.1, 7.6, and 12.4 °C, respectively, and enantiotropic N* and Sc* phases. A chiral smectic F phase is observed for the PSn12C series except for PS312C. Additionally, for PS012C a blue phase is

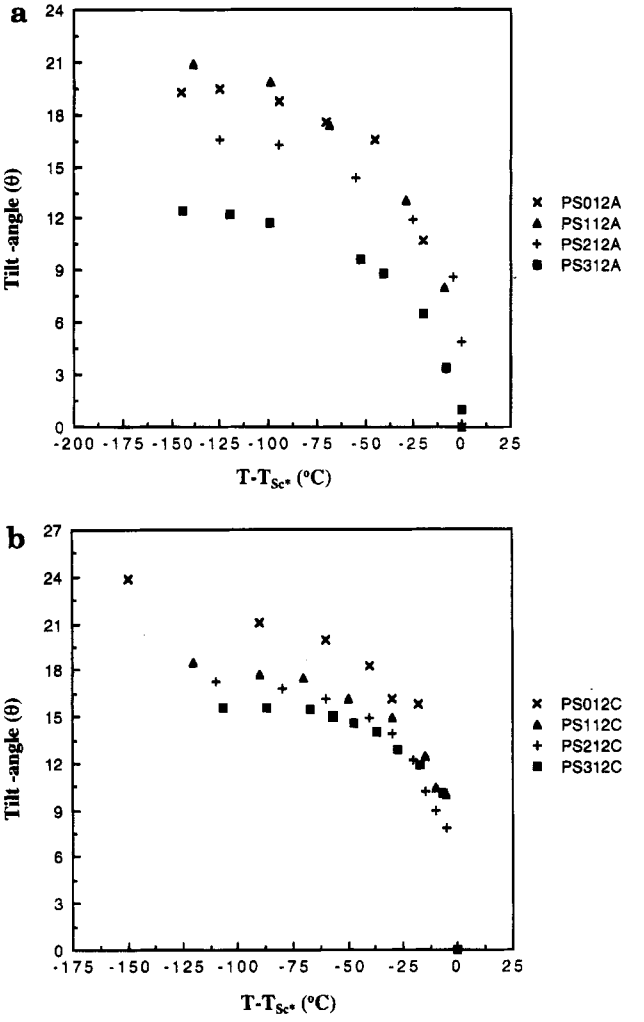

Figure 6. Plots of tilt angle versus ΔT ($T - T_{Sc*}$): (a) polymer PSn12A series, (n = 0, ×), (n = 1, ▲), (n = 2, +), (n = 3, ■); (b) polymer PSn12C series, (n = 0, ×), (n = 1, ▲), (n = 2, +), (n = 3, ■).

observed upon cooling from the isotropic liquid (Figure 11a. Figure 12 presents representative temperature-dependent X-ray diffraction diagrams for PS112C. Curve A and the optical polarizing micrograph of Figure 11b are both consistent with a cholesteric phase. Both curve B and curve C show small-angle reflections at 28.0506 and 27.3996 Å, respectively. The d-spacing versus measuring temperature is presented in Figure 5c. As shown in this figure, the d-spacing decreases as the temperature decreases below the cholesteric point. On the other hand, a broken fan texture observed for PS112C at 173.9 °C is shown in Figure 11c. These results are in agreement with the formation of a chiral smectic C phase since the tilt angle of the side chains generally increases with decreasing temperature for a chiral smectic C side chain LCP. Figure 6b reveals the tilt angle versus temperature difference of $T - T_{Sc*}$ for the PSn12C series. The tilt angle was calculated from eq 2 due to the absence of a smectic A phase in the PSn12C series.

$$\theta = \cos^{-1}\left(\frac{d_{Sc*}}{d_{Sc*(Max)}}\right) \qquad (2)$$

The $d_{Sc*(Max)}$ value was selected from the maximum layer spacing of the chiral smectic C phase. The maximum tilt angle presented here is about 24° for PS012C. Curve D shows a small-angle reflection at

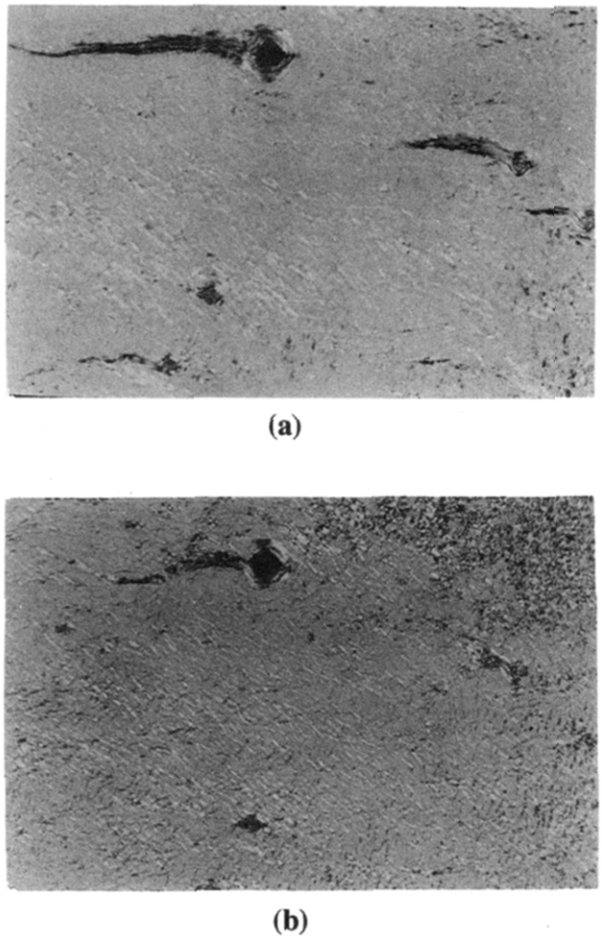

Figure 7. Optical polarizing micrographs shown by PS012A (n = 0): (a) iridescent cholesteric-like texture of TGB_A phase at 192.1 °C (400x); (b) cholesteric phase with oily streaks at 179.2 °C (400x).

Table 3. Phase Transitions and Phase Transition Enthalpies for Polymer Series PSn12B

polymer	n[a]	heating / cooling phase transitions, °C (corresponding enthalpy changes; kcal/mru)[b]
PS012B	0	G 27 I / I 20 G
PS112B	1	G 10.2 S_A 150(0.457) I / I 132(0.5) S_A 10.7 G
PS212B	2	G −5.0 TGB_A 122.7(0.526) I / I 117.5(0.625) TGB_A 0.3 G
PS312B	3	G −0.4 TGB_A 100(−)[c] N* 112(0.737) I / I 101.7(−)[d] N* 94.6(0.649) TGB_A 11 G

[a] n according to Scheme 2. [b] mru = mole repeating unit, G = glassy, S_A = smectic A, TGB_A = twist grain boundary A, N* = cholesteric, I = isotropic. [c] The transition was decided by POM. [d] ΔH(TGB_A−N*−I).

27.0865 Å and a sharp wide-angle reflection at 4.511 Å. This indicates the formation of the hexagonal structure of the chiral smectic F phase. Figure 11d displays the chiral smectic F phase at 37.3 °C. A comparison of the thermal transitions of polymer series PSn11A, PSn12A, PSn12B, and PSn12C reveals that a flexible polysiloxane backbone has a tendency of have a lower glass transition and a wider mesomorphic temperature range. The phase behaviors of the PSn12A,

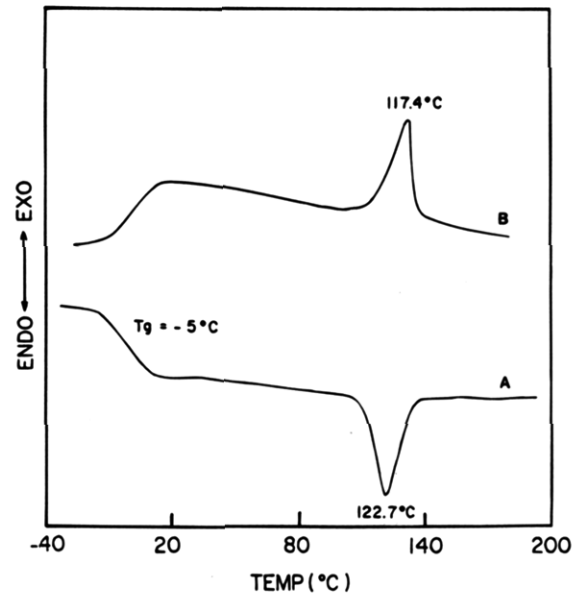

Figure 8. DSC thermogram (10 °C/min) of polymer PS212B (n = 2): (A) second heating scan; (B) cooling scan.

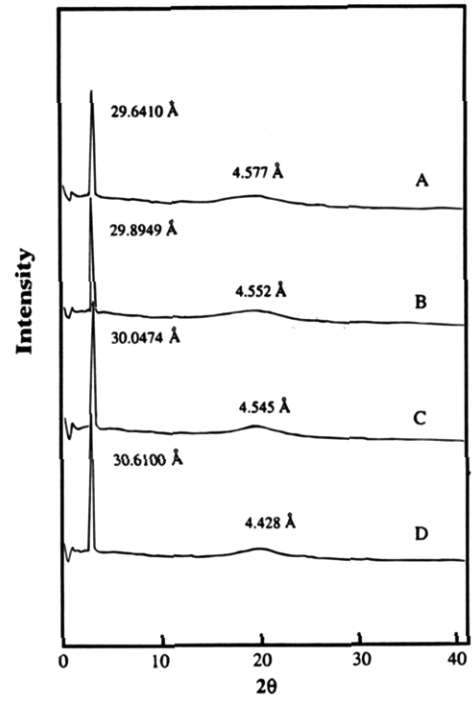

Figure 9. Temperature-dependent X-ray measurements for polymer PS212B with two oxyethylene spacers at (A) 103, (B) 75, (C) 61, and (D) 25.6 °C.

PSn12B, and PSn12C series can be compared by superimposing the plots of the dependencies of their thermal transition temperatures shown in Figure 2 as a function of the number of oxyethylene spacer units (n). The PSn11A series reveals the presence of a viscous liquid, and this series is not liquid crystalline due to the more flexible polymer backbone and oxyethylene spacers in the phenyl benzoate mesogenic system. However, PSn12A, PSn12B, and PSn12C present good liquid crystalline thermal properties in light of the fact that the flexible polymer backbone and oxyethylene spacer in the more rigid three aromatic ring ester system (biphenyl benzoate mesogenic group) reach a suitable balance for the formation of liquid crystalline structures. Nevertheless, the chiral butyl tails ((2*S*)-2-methyl-1-butyl and (2*S*, 3*S*)-(2-chloro-3-methylpentanoyl)oxy) are

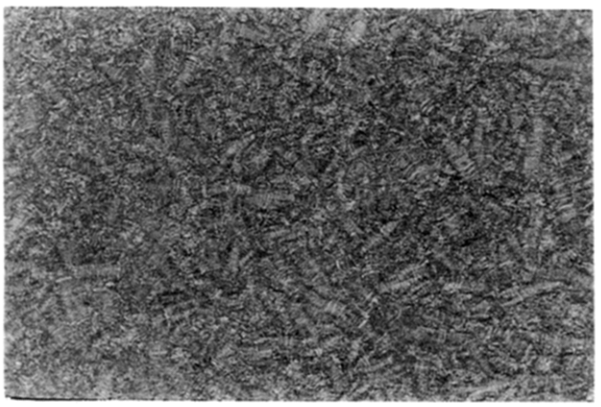

Figure 10. Optical polarizing micrographs displayed by polymer PS212B ($n = 2$) at 109.2 °C: filament texture of twist grain boundary A phase (500x).

more inclined to form a chiral smectic C phase than a longer chiral heptyl ((2*R*)-1-methylheptyl) in the flexible polymer backbone/oxyethylene spacers and three aromatic ring ester system. We believe that the (2*R*)-1-methylheptyl chiral tail would be suitable for formation of the chiral smectic C phase in the four aromatic ring ester system, biphenyl biphenylcarboxylate mesogenic group. These results will be published in a future work.

In conclusion, four series of new side chain liquid crystalline polysiloxanes containing oligo(oxyethylene), phenyl benzoate/biphenyl benzoate mesogens, and three different kinds of chiral moieties ((2*S*)-2-methyl -1-butyl, (2*R*)-1-methylheptyl, and (2*S*, 3*S*)-(2-chloro-3-methylpentanoyl)oxy) have been synthesized. The series PS*n*12A, PS*n*12B, and PS*n*12C with biphenyl benzoate mesogenic groups exhibit smectic mesomorphism. A twist grain boundary A phase was found in some compounds, PS012A, PS212B, and PS312B. The intermediary twist grain boundary phase apparently has a structure where a helical ordering of the molecules has occurred in the plane of the molecular layer. Among the three polymer series, two series (PS*n*12A and

Table 4. Phase Transitions and Phase Transition Enthalpies for Polymer Series PS*n*12C

polymer	n[a]	heating / cooling phase transitions, °C (corresponding enthalpy changes; kcal/mru)[b]
PS012C	0	G 22.2 S_F* −[d] Sc* 197.5(−) N* 225(0.129)[e] I / I 210[c] BP 205.9 N* 190.5(0.24)[e] Sc* 44(−)[f] S_F* 20 G
PS112C	1	G 20.1 S_F* −[d] Sc* 204.4(−) N* 218(0.457)[e] I / I 202(−) N* 195.1(0.554)[e] Sc* 55(−)[f] S_F* 15.6 G
PS212C	2	G 7.6 S_F* −[d] Sc* 197.6(−) N* 204(0.533)[e] I / I 190(−) N* 182.2(0.518)[e] Sc* 65(−)[f] S_F* 19.4 G
PS312C	3	G 12.4 Sc* 171.3 N* 173(0.867)[e] I / I 160.5(−) N* 150(0.808)[e] Sc* 5.3 G

[a] n according to Scheme 2. [b] mru = mole repeating unit, G = glassy, S_F* = chiral smectic F, S_A = smectic A, Sc* = chiral smectic C, N* = cholesteric, I = isotropic. [c] The transition was decided by POM. [d] The transition was difficult to detect. [e] ΔH(Sc*−N*−I). [f] The transition enthalpies were too small to evaluate.

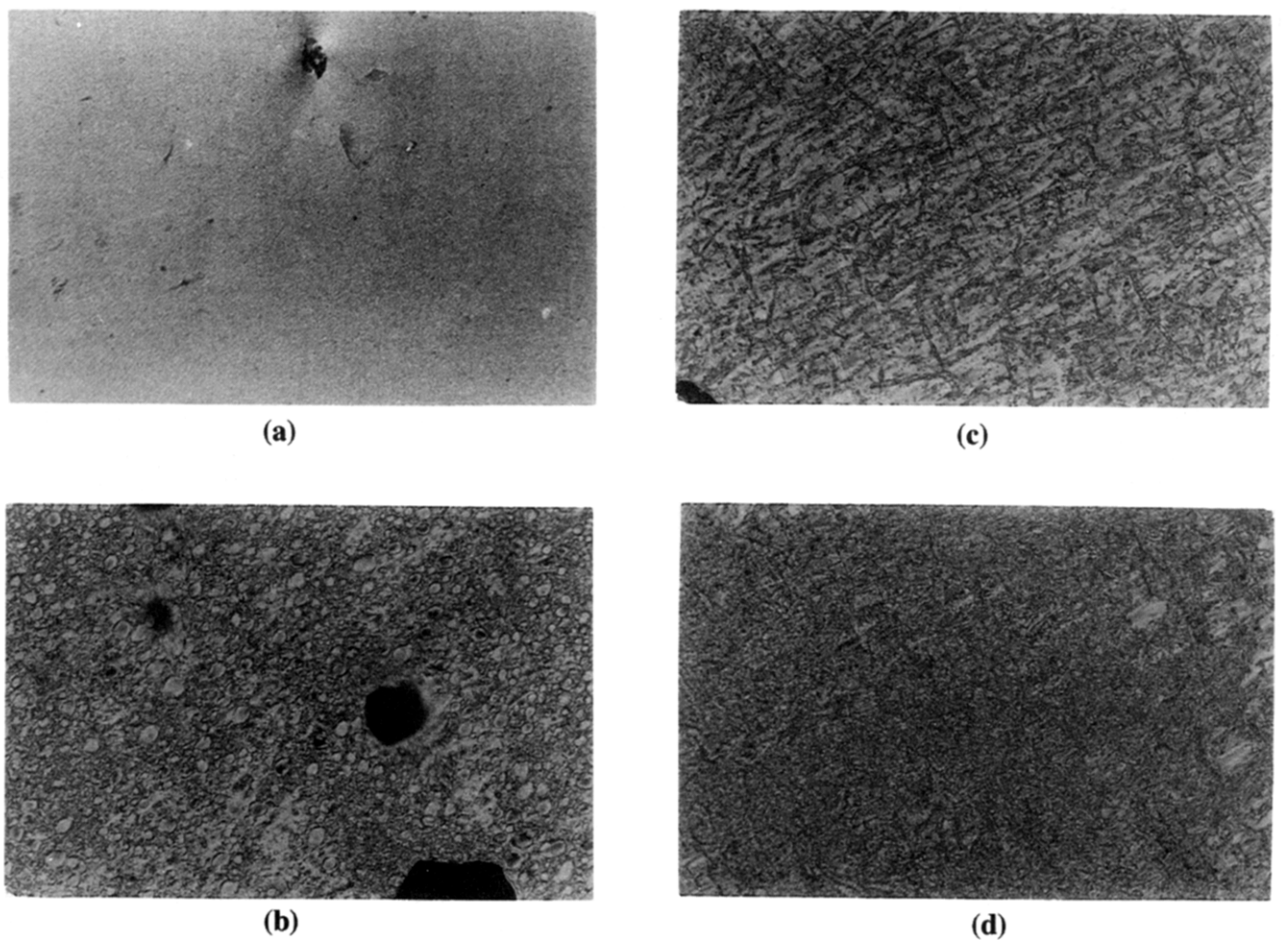

Figure 11. Optical polarizing micrographs: (a) blue phase of PS012C at 208.3 °C (400x); (b) cholesteric phase of PS112C at 204.4 °C (400x); (c) chiral smectic C phase of PS112C at 173.9 °C (400x); (d) chiral smectic F phase of PS112C at 37.3 °C (400x).

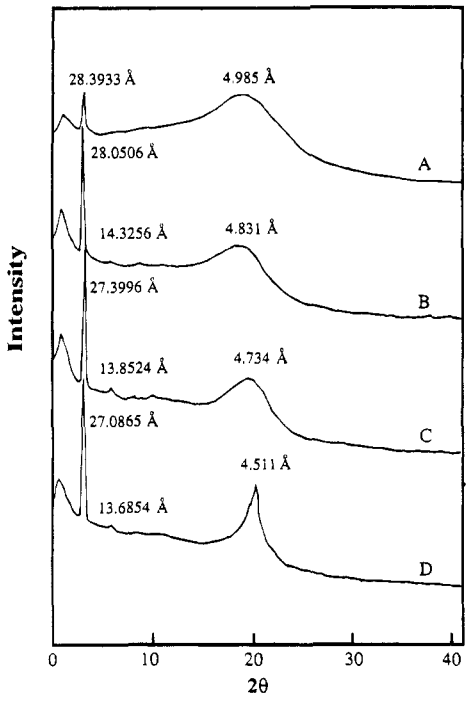

Figure 12. Temperature-dependent X-ray diffraction measurements for polymer PS112C with one oxyethylene spacer at (A) 200, (B) 180, (C) 140, and (D) 40 °C.

PS*n*12C) with chiral butyl moieties reveal a wide temperature range of the chiral smectic C phase. The rigidity of the aromatic ring ester core plays an essential role in the formation of mesophases. The flexibility of the chiral tail has a significant effect on the thermal stability of the chiral smectic C phase. A flexible polymer backbone enhances the decoupling of the motions of the side chain and the main chain and thereby tends to give rise to a higher thermal stability of the mesophases, including the chiral smectic C phase.

Acknowledgment. The authors are grateful to the National Science Council of the Republic of China for financial support of this work (Grants NSC-82-0511-E007-01 and NSC-83-0511-E007-01).

References and Notes

(1) Meyer, R. B.; Liebert, L.; Strzelecki, L.; Keller, P. *J. Phys. Lett.* **1975**, *36*, 69.
(2) Clark, N. A.; Lagerwall, S. T. *Appl. Phys. Lett.* **1980**, *36*, 898.
(3) Leslie, T. M. *Ferroelectrics* **1984**, *58*, 9.
(4) Furukawa, K.; Terashima, K.; Ichihashi, M.; Inoue, H.; Saito, S.; Inukai, T. *6th Liq. Cryst. Conf. Soc. Count.*, Halle (GDR), Abstract, **1985**, A37, 1985.
(5) Furukawa, K.; Terashima, K. Eur. Pat. Appl. EP 178,647, 1986.
(6) Keller, P. *Mol. Cryst. Liq. Cryst.* **1984**, *102*, 295.
(7) Koden, M.; Katsuse, H.; Itoh, N.; Kaneko, T.; Tamai, K.; Takeda, H.; Shiomi, M.; Numao, N.; Kido, M.; Matsuki, M.; Miyoshi, S.; Wada, T. *Abstracts of Fourth International Conference on Ferroelectric Liquid Crystals* **1993**, p-146, 369.
(8) Tajima, E.; Kondoh, S.; Suzuki, Y. *Abstracts of Fourth International Conference on Ferroelectric Liquid Crystals* **1993**, p-147, 371.
(9) Shibaev, V. P.; Beresnev, L. A.; Blinov, L. M.; Kozlovsky, M. V.; Plate, N. A. *Polym. Bull.* **1984**, *12*, 299.
(10) Decobert, G.; Soyer, F.; Dubois, J. C. *Polym. Bull.* **1985**, *14*, 179.
(11) Decobert, G.; Dubois, J. C.; Esselin, S.; Noel, C. *Liq. Cryst.* **1986**, *1*, 307.
(12) Zentel, R.; Reckert, G.; Reck, B. *Liq. Cryst.* **1987**, *2*, 83.
(13) Hahn, B.; Percec, V. *Macromolecules* **1987**, *20*, 2961.
(14) Bualek, S.; Kapitza, H.; Meyer, J.; Schmidt, G. F.; Zentel, R. *Mol. Cryst. Liq. Cryst.* **1988**, *155*, 47.
(15) Esselin, S.; Noel, C.; Decobert, G.; Dubois, J. C. *Mol. Cryst. Liq. Cryst.* **1988**, *155*, 371.
(16) Vallerien, S. U.; Zentel, R.; Kremer, F.; Kapitza, H.; Fischer, E. W. *Makromol. Chem., Rapid Commun.* **1989**, *10*, 333.
(17) Scherowsky, G.; Schliwa, A.; Springer, J.; Kuhnpast, K.; Trapp, W. *Liq. Cryst.* **1989**, *5*, 1281.
(18) Shibaev, V. P.; Kozlovsky, M. V.; Plate, N. A.; Beresnev, L. A.; Blinov, L. M. *Liq. Cryst.* **1990**, *8*, 545.
(19) Dumon, M.; Nguyen, H. T.; Mauzac, M.; Destrade, C.; Achard, M. F.; Gasparoux, H. *Macromolecules* **1990**, *23*, 355.
(20) Vallerien, S. U.; Kremer, F.; Fischer, E. W.; Kapitza, H.; Zentel, R.; Poths, H. *Makromol. Chem., Rapid Commun.* **1990**, *11*, 593.
(21) Vallerien, S. U.; Kremker, F.; Kapitza, H.; Zentel, R.; Fischer, E. W. *Ferroelectrics* **1990**, *109*, 273.
(22) Brand, H. R.; Pleiner, H. *Makromol. Chem., Rapid. Commun.* **1990**, *11*, 607.
(23) Endo, H.; Hachiya, S.; Uchida, S.; Hashimoto, K.; Kawasaki, K. *Liq. Cryst.* **1991**, *9*, 635.
(24) Kapitza, H.; Zentel, R. *Makromol. Chem.* **1991**, *192*, 1859.
(25) Bomelburg, J.; Heppke, G.; Hollidt, J. *Makromol. Chem., Rapid. Commun.* **1991**, *12*, 483.
(26) LeBarny, P.; Dubois, J. C. In *Side Chain Liquid Crystal Polymers*; McArdle, C. B., Ed.; Blackie: Glasgow, London, 1989; p 130.
(27) Hsu, C. S.; Lin, J. H.; Chou, L. R.; Hsiue, G. H. *Macromolecules* **1992**, *25*, 7126.
(28) Hsu, C. S.; Shih, L. J.; Hsiue, G. H. *Macromolecules* **1993**, *26*, 3161.
(29) Wu, S. L.; Hsieh, W. J.; Chen, D. G.; Chen, S. J.; Shy, J. T.; Hsiue, G. H. *Mol. Cryst. Liq. Cryst.*, accepted.
(30) Chen, J. H.; Chang, R. C.; Guu, F. W.; Hsiue, G. H.; Wu, S. L. *Liq. Cryst.* **1995**, *18*, 291.
(31) Benattar, J. J.; Doucet, J.; Lambert, M.; Levelut, A. M. *Phys. Rev. A* **1979**, *20*, 2505.
(32) Chen, J. H.; Chang, R. C.; Hsiue, G. H. *Ferroelectrics* **1993**, *147*, 241.
(33) Nguyen, H. T.; Twieg, R. T.; Nabor, M. F.; Isaert, N.; Destradem, C. *Ferroelectrics* **1991**, *121*, 187.
(34) Goodby, J. W.; Waugh, M. A.; Stein, S. M.; Chin, E.; Pindak, R.; Patel, J. S. *Nature (London)* **1989**, *337*, 449.
(35) Navailles, L.; Nguyen, H. T.; Barois, P.; Destrade, C.; Isaert, N. *Liq. Crys.* **1993**, *15*, 479.

MA950015V